Suppression of Torque Ripple Caused by Misalignment of the Gearbox by Using Harmonic Current Injection Method

Soo-Hwan Park, Jin-Cheol Park, Sung-Woo Hwang, Jae-Hyun Kim, Hyeon-Jin Park, and Myung-Seop Lim, *Member, IEEE*

***Abstract*—This article proposes a method to suppress the torque ripple caused by misalignment of the gearbox. Misalignment is a common fault caused by the manufacturing tolerances, and generates torque ripple. Therefore, even if a constant electromagnetic torque is transmitted from the motor to the gearbox, a large torque ripple may be transmitted to the load because of misalignment. In the proposed method, a harmonic current injection method, in which harmonic current is injected into the armature current, is used to suppress the torque ripple produced by misalignment. The amplitude and phase of the harmonic current are calculated using the misalignment torque ripple, and a method for estimating the misalignment torque ripple, which does not require a torque sensor, has been presented. Using the estimation method and harmonic current injection method, the misalignment torque ripple can be suppressed effectively. The phenomenon of torque ripple production by misalignment is analyzed, and a current control algorithm based on harmonic current injection method is proposed. The effectiveness of the proposed method is verified through experiments at various load torque. Using this method, a high degree of torque control can be achieved with even a low-quality gearbox.**

***Index Terms*—Harmonic current injection method, misalignment, robotics actuator, torque control, torque ripple suppression.**

I. Introduction

THE LOW TORQUE ripple of a surface-mounted permanent magnet synchronous motor (SPMSM) is an outstanding solution for achieving high-precision control without using expensive sensors or controllers [1]. Therefore, the SPMSMs are widely used in mechatronic systems, such as multiaxis industrial robots or wearable robots [2], [3]. The main goal of a mechatronic system is to control the load precisely according to user requirements. In general, mechatronic systems consist of a controller, an actuator, and the load. The actuator comprises a gearbox, SPMSM, and position sensor. The SPMSM is designed to have a sinusoidal back electromotive force (back EMF) to generate electromagnetic torque with low torque ripple. Nevertheless, high torque ripple is often generated and transmitted to the load because of various irregularities arising from the manufacturing tolerances of components in the gearbox. Among such reasons, shaft misalignment is the most common cause of failure in rotating machinery, and it causes high torque ripple and reduces the lifetimes of the bearings [4], [5]. As torque control is mainly used in robot manipulation, torque ripple due to misalignments often degrade the performance of the robots [6]. Therefore, it is necessary to eliminate such torque ripples to improve the performance of torque control.

Methods to reduce the torque ripple caused by misalignments can be broadly classified into two types. The first type controls the manufacturing tolerances of the gearbox. However, these methods incur high cost and require much effort, for example, expensive machining tools or highly experienced engineers may be necessary. Therefore, more efficient methods to reduce the torque ripple are necessary. The second type controls the SPMSM instead of controlling the manufacturing tolerances. In this article, a harmonic current injection method is adopted to suppress the torque ripple. Fig. 1 shows the strategy for the proposed method. Using the proposed method, the misalignment torque ripple can be suppressed by injecting an electromagnetic torque ripple into the SPMSM, wherein the injected phase is opposite to that of the misalignment torque ripple.

The harmonic current injection method has been widely used in power converter applications because it is useful for eliminating specific harmonic components in the torque ripple. In [7]–[9], the torque ripples of various motors, such as the permanent magnet synchronous motor and variable flux reluctance motor, were reduced using this method. As the inductances and flux-linkages vary with the extent of the magnetic saturation, the amplitudes and phases of the injected harmonic currents are determined by considering these parameter variations [10].

Manuscript received January 8, 2020; revised March 26, 2020; accepted April 29, 2020. Date of publication June 2, 2020; date of current version August 13, 2020. This work was supported in part by the National Research Foundation of Korea (NRF) and in part by the Korea government (MSIP; Ministry of Science, ICT & Future Planning) under Grant 2018R1C1B5085447. Recommended by Technical Editor T. Shimono and Senior Editor X. Chen. *(Corresponding author: Myung-Seop Lim.)*

The authors are with the Department of Automotive Engineering, Hanyang University, Seoul 04763, South Korea (e-mail: shwanp14@hanyang.ac.kr; skensk1990@hanyang.ac.kr; supertramph@hanyang.ac.kr; zerg1258@hanyang.ac.kr; hjpark@katech.re.kr; myungseop@hanyang.ac.kr).

Color versions of one or more of the figures in this article are available online at https://ieeexplore.ieee.org.

Digital Object Identifier 10.1109/TMECH.2020.2999379

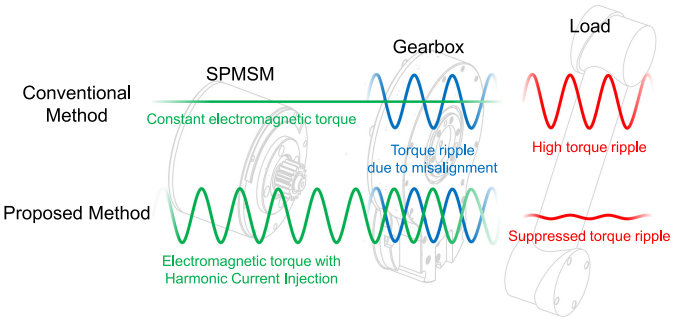

Fig. 1. Strategy for the proposed method.

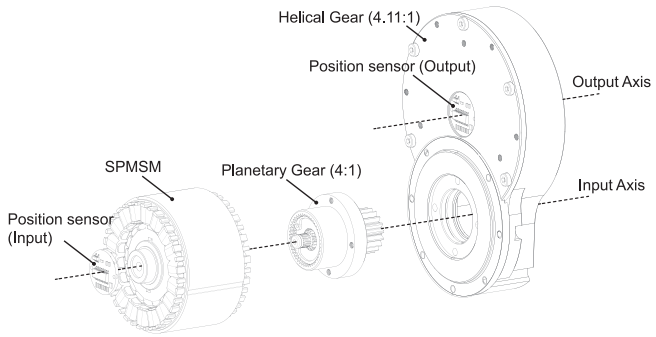

Fig. 2. Configuration of the actuator for wearable robot.

However, the aforementioned studies used the harmonic current injection method to reduce the electromagnetic torque ripple and did not consider the torque ripple in mechatronic systems. Kim *et al.* and Godler *et al.* proposed methods to compensate the torque ripple caused by the gearbox [11], [12]. However, these methods were based on torque sensors embedded in the mechatronic systems, such methods were inefficient as they required high cost and maintenance. It is more advantageous to suppress misalignment torque than suppressing electromagnetic torque as the control performance can be improved without using an additional torque sensor.

This article is organized as follows. In Section II, the effect of the shaft misalignment on the torque ripple has been analyzed. In Section III, the harmonic current injection method and the strategy to implement the method for suppressing the misalignment torque ripple have been proposed. In Section IV, the estimation method of the misalignment torque ripple without torque sensor have been presented. The experimental verification of the proposed method has been described in Section V. Finally, Section VI concludes this article.

II. Torque Ripple Caused by the Misalignment in Gearbox

A. Torque Ripple Generated in Actuator

Fig. 2 shows the exploded view of the actuator. The actuator has two-stage gearbox whose overall gear ratio is 16.44:1, SPMSM that has 16 poles, 18 slots, and position sensors for feedback. Table I presents the specifications of each component in the actuator for wearable robot.

TABLE I
Specifications of the Actuator for Wearable Robot

Item	Unit	Value
Number of poles	-	16
Number of slots	-	18
DC link voltage	V	24
Max. power	W	100
Rated torque (Input)	Nm	0.5 (1.0 p.u.)
Max. speed (Input)	rpm	1,100 (1.0 p.u.)
Rated torque (Output)	Nm	8 (1.0 p.u.)
Max. speed (Output)	rpm	65
Phase resistance (R_a)	Ω	0.58
d-axis inductance (L_d)	mH	1.44
q-axis inductance (L_q)	mH	1.47
Flux-linkage (ψ_a)	Wb	0.024
Overall gear ratio	-	16.44:1

TABLE II
Causes of the Torque Ripple Included in Actuator

Reference frequency	Harmonic component	Cause
Motor shaft	1st	Misalignment of stator and rotor
Motor shaft	144th	Cogging torque caused by pole and slot combination
Motor shaft	16th, 32th, ...	Cogging torque caused by stator tolerances
Motor shaft	18th, 36th, ...	Cogging torque caused by rotor tolerances
Armature current	6th, 12th, ...	Torque ripple
Gearbox output shaft	1st, 2nd, 3rd, ...	Shaft misalignment
Gearbox output shaft	near in 74th	Friction in gearbox

Table II lists causes of the torque ripple in the actuator. The causes are divided into the electromagnetic and mechanical phenomena. The torque ripple by electromagnetic phenomena is classified into the cogging torque and electromagnetic torque ripple. Since the manufacturing tolerances inevitably occur, the 16th and 18th multiples referred in the frequency of the motor shaft, which are concerned with the number of poles and slots, can be generated [13]. The cogging torque of the 144th order basically occurs in 16 poles and 18 slots SPMSM. In addition, the torque ripple of 6th multiples referred in the electrical frequency can be loaded on the electromagnetic torque because of the interaction between the flux-linkage and armature current. Then, the electromagnetic torque can be expressed as the sum of averaged torque and torque ripple

$$T_e = \bar{T}_e + \sum_n T_{e,n} \cos\left(nN_g\theta_{\text{out}} + \phi_{e,n}\right) \tag{1}$$

where T_e is the electromagnetic torque, $\bar{T}_e$ and $T_{e,n}$ are the averaged torque and amplitude for the nth electromagnetic torque, respectively, n and N_g are the harmonic orders referred in the output shaft and gear ratio, and θ_{out} and $\phi_{e,n}$ are the position

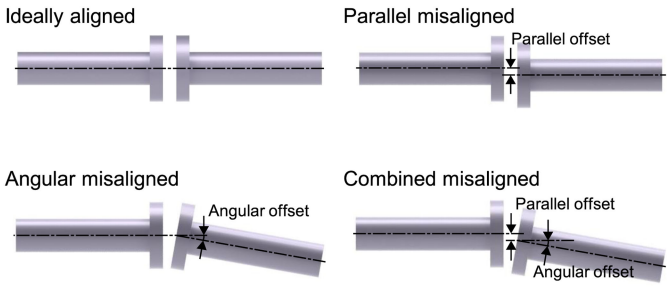

Fig. 3. Types of shaft misalignment.

of the output shaft and phase offset for the nth electromagnetic torque, respectively.

The torque ripples caused by mechanical phenomena can be classified into torque ripples caused by misalignments and those caused by the gear meshing. Misalignments are common problems caused by manufacturing tolerances. Fig. 3 shows the types of misalignments. Misalignments in gearboxes generally occur when the shafts are connected with parallel or angular offsets. As the manufacturing of the gearbox involves several processes such as forming, machining, and finishing, manufacturing tolerances variations may occur inevitably. In addition, it is difficult to align the shafts in the target actuator because the actuator comprises several shafts. Thus, such misalignments cause torque ripples at multiples (1st, 2nd, 3rd, etc.) and at the sidebands referred in the frequency of the output shaft [14], [15]. The torque ripple caused by the gear meshing can be observed at multiples of the gear meshing frequency, which is defined as the product of the number of teeth and the rotating speed. These torque ripples can be expressed as the friction torque because they are caused by the friction generated in the bearing because of misalignment and that generated in the gearbox because of the gear meshing [16], [17]. Then, the friction torque can be expressed as

$$T_f = B\bar{\omega}_{\text{out}} + B\sum_n \omega_{\text{out},n}\cos\left(n\theta_{\text{out}} + \phi_{f,n}\right) \tag{2}$$

where T_f and B are the friction torque and friction coefficient, respectively, $\bar{\omega}_{\text{out}}$ is the averaged rotating speed of output shaft, $\omega_{\text{out},n}$ and $\phi_{f,n}$ are the amplitude for nth rotating speed of output shaft and phase offset for nth friction torque, respectively.

B. Rotor Dynamics by the Torque Ripple in Actuator

Since the rotating machinery is driven by the output torque, which is the electromagnetic torque amplified by the gearbox, the output torque can be reduced by the friction and load torque. Then, the acceleration in output shaft can be determined by following equation of motion:

$$\frac{d\omega_{\text{out}}}{dt} = \frac{1}{J_{\text{eq}}}(T_e N_g - T_f - T_l) \tag{3}$$

where T_l and J_{eq} are the load torque and equivalent moment of inertia referred in output shaft, respectively. When the averaged rotating speed is in a steady state, the averaged output torque is equal to the sum of averaged friction torque, and load torque. Then, the output shaft is accelerated by the torque ripple of each component as

$$\frac{d\omega_{\text{out}}}{dt} = \frac{1}{J_{\text{eq}}}\left\{N_g\sum\nolimits_n T_{e,n}\cos\left(nN_g\theta_{\text{out}} + \phi_{e,n}\right) - B\sum\nolimits_n \omega_{\text{out},n}\cos\left(n\theta_{\text{out}} + \phi_{f,n}\right)\right\}. \tag{4}$$

Since the acceleration is a time derivative of the rotating speed, the rotating speed contains the same harmonic components with the acceleration. The misalignment torque ripple is defined as the sum of electromagnetic torque ripple and friction torque ripple as

$$T_{\text{mis}} = N_g\sum_n T_{e,n}\cos\left(nN_g\theta_{\text{out}} + \phi_{e,n}\right) - B\sum_n \omega_{\text{out},n}\cos\left(n\theta_{\text{out}} + \phi_{f,n}\right) \tag{5}$$

where T_{mis} is the misalignment torque ripple. As the misalignment torque ripple is difficult to be reduced by manufacturing the gearbox without any misalignment, it is efficient to use the control method for suppressing the torque ripple.

III. Torque Ripple Suppression Using Harmonic Current Injection Method

A. Electromagnetic Torque With Harmonic Current Injection

The ideal electromagnetic torque is generated by the interaction of sinusoidal three-phase flux-linkage and armature current. The flux-linkage and armature current can be expressed based on the d- and q-axis, and the performance of the SPMSM can be calculated by using the d- and q-axis voltage equations. In the voltage equations, the eddy current loss in permanent magnets is omitted because it can be negligible in the SPMSM, which has 16 poles and 18 slots [18]. The d- and q-axis voltage equations can be expressed as

$$\begin{bmatrix} v_d \\ v_q \end{bmatrix} = R_a\begin{bmatrix} i_{od} \\ i_{oq} \end{bmatrix} + \left(1 + \frac{R_a}{R_c}\right)\begin{bmatrix} v_{od} \\ v_{oq} \end{bmatrix} + p\begin{bmatrix} L_d & 0 \\ 0 & L_q \end{bmatrix}\begin{bmatrix} i_{od} \\ i_{oq} \end{bmatrix} \tag{6}$$

$$\begin{bmatrix} v_{od} \\ v_{oq} \end{bmatrix} = \begin{bmatrix} 0 & -\omega_e L_q \\ \omega_e L_d & 0 \end{bmatrix}\begin{bmatrix} i_{od} \\ i_{oq} \end{bmatrix} + \begin{bmatrix} 0 \\ \omega_e\psi_a \end{bmatrix} \tag{7}$$

$$R_c = \frac{\omega_e^2\left(v_{od}^2 + v_{oq}^2\right)}{W_i} \tag{8}$$

$$i_{cd} = -\frac{v_{od}}{R_c},\ i_{cq} = \frac{v_{oq}}{R_c} \tag{9}$$

where the subscripts of d and q are the d- and q-axis, respectively, p is the differential operator as d/dt, v_d and v_q are the terminal voltages, v_{od} and v_{oq} are the induced voltages, i_{od} and i_{oq} are the magnetization currents, R_a is the phase resistance, L_d and L_q are the d- and q-axis inductances, respectively, ψ_a is the flux-linkage by permanent magnets, ω_e is the electrical rotating speed, W_i is the iron loss, R_c is the iron loss resistance, and the i_{cd} and i_{cq} are the iron loss currents. Then, the d- and q-axis

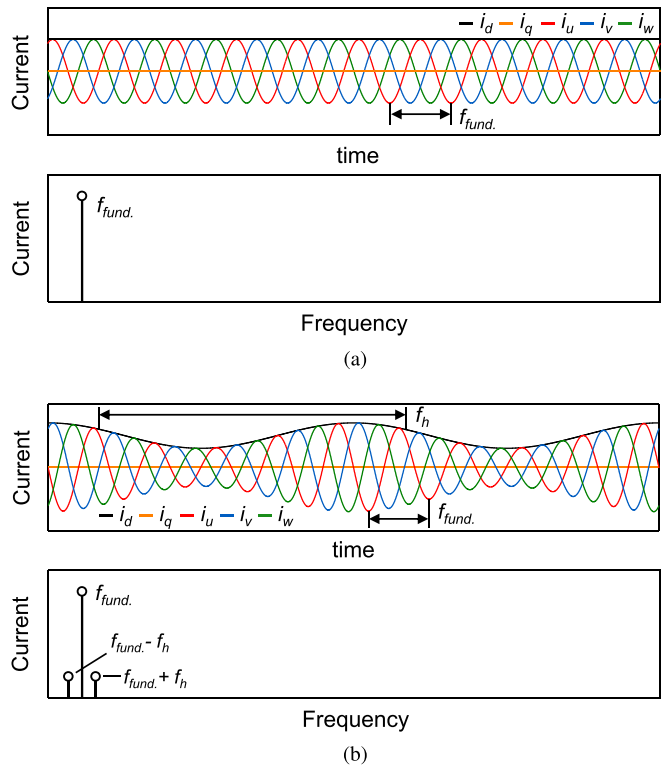

Fig. 4. Waveform and harmonic analysis of three-phase armature current (a) without and (b) with harmonic current injection.

currents can be calculated as

$$i_d = i_{od} + i_{cd},\ i_q = i_{oq} + i_{cq} \tag{10}$$

where i_d and i_q are the d- and q-axis currents, respectively. Since the electromagnetic torque is only generated by the magnetizing currents, the electromagnetic torque can be expressed as

$$T_e = 1.5P_r \left\{\psi_a i_{oq} + (L_d - L_q)\, i_{od} i_{oq}\right\} \tag{11}$$

where P_r is the pole-pair. Since the reluctance torque cannot be expected in the SPMSM, current vector control method of "$i_d = 0$" is adopted. When the SPMSM is controlled with the current vector control method of "$i_d = 0$," i_{od} can be generated to cancel i_{cd}. Since i_{od} cannot be measured in motor drive, i_d is controlled to be zero instead of controlling i_{od}. Since the reluctance torque that is generated by i_{od} is much smaller than the magnetic torque, the electromagnetic torque can be expressed as

$$T_e = 1.5P_r \psi_a i_{oq}. \tag{12}$$

Thus, the electromagnetic torque has no torque ripple when the three-phase back EMF and armature current are completely sinusoidal.

As the electromagnetic torque is controlled by the i_q, not i_{oq}, the harmonic current injected i_q can be expressed as

$$i_q = \bar{i}_q + \sum_n i_{q,n} \cos\left(n\theta_{\text{out}} + \phi_{q,n}\right) \tag{13}$$

where $\bar{i}_q$ is the averaged q-axis current, and $\phi_{q,n}$ is the phase offset for the nth q-axis current. Fig. 4(a) and (b) shows the waveform of three-phase armature current and d- and q-axis current with/without harmonic current injection. When the harmonic current that has frequency near in output rotating speed is injected into the q-axis current, the phase current is modulated by the amplitude of the injected harmonic current. Since the iron loss is generated in the SPMSM, the electromagnetic torque is only generated by the q-axis magnetization current, which is reduced by the q-axis iron loss current from the q-axis current. Thus, the harmonic current injected i_{oq} can be expressed as

$$\begin{aligned} i_{oq} &= i_q - i_{cq} \\ &= \bar{i}_{oq} + \sum_n i_{oq,n} \cos\left(n\theta_{\text{out}} + \phi_{oq,n}\right) \end{aligned} \tag{14}$$

where $\bar{i}_{oq}$ is the averaged q-axis magnetization current, and $i_{oq,n}$, $\phi_{oq,n}$ are the amplitude and phase for the nth q-axis harmonic magnetization current. Since the iron loss is affected by the magnetic flux density and frequency, i_{cq} can be varied with i_q and rotating speed. Then, the electromagnetic torque with harmonic currents can be obtained by substituting (14) into (12) as

$$T_e = 1.5P_r\psi_a \left\{\bar{i}_{oq} + \sum\nolimits_n i_{oq,n} \cos\left(n\theta_{\text{out}} + \phi_{oq,n}\right)\right\}. \tag{15}$$

Therefore, the electromagnetic torque ripple can be produced intentionally by injecting harmonic currents into the q-axis current.

The harmonic current generates additional copper and iron losses, and decreases the efficiency. The additional copper loss is affected by the amplitude of the injected harmonic current, and the iron loss is affected by the amplitude and frequency of the injected harmonic current. As the frequency of the injected phase current is close to the fundamental frequency of phase current, as shown in Fig. 4(b), the additional iron loss depends on the amplitude of the injected q-axis current. Consequently, the decrease in efficiency is dependent on the amplitude of the injected q-axis current. However, the decrease in the efficiency may not be significant when the amplitude of the injected q-axis current is small.

B. Scheme of the Proposed Method

Fig. 5 shows the process for suppressing the misalignment torque ripple. As the performance of the proposed method depends on the injected harmonic current, it is important to determine the amplitude and phase of the harmonic current. The amplitude and phase are determined via the compensation torque, which is calculated from the misalignment torque ripple. The detailed process is shown as follows:

1) Step 1: The misalignment torque ripple is estimated to calculate the compensation torque when the rotating speed is in the steady state. The steady state can be achieved by controlling the q-axis current and load constantly. The estimation method for the misalignment torque ripple is described in Section IV.
2) Step 2: After the estimation of the misalignment torque ripple, the harmonic analysis is conducted. Because the compensation torque is determined by the sum of the various torque ripple components, the misalignment torque

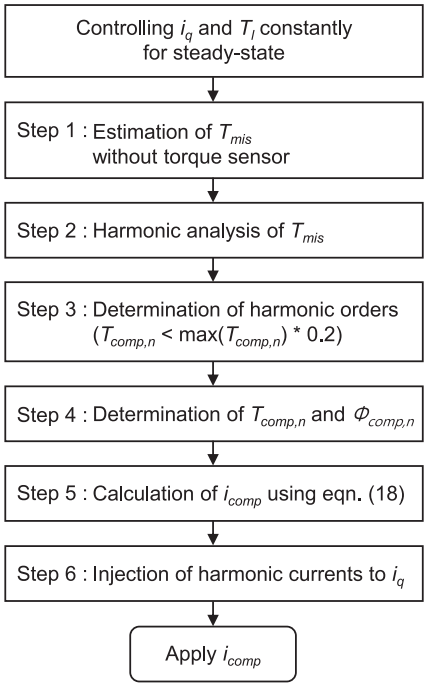

Fig. 5. Flowchart for implementing the proposed method.

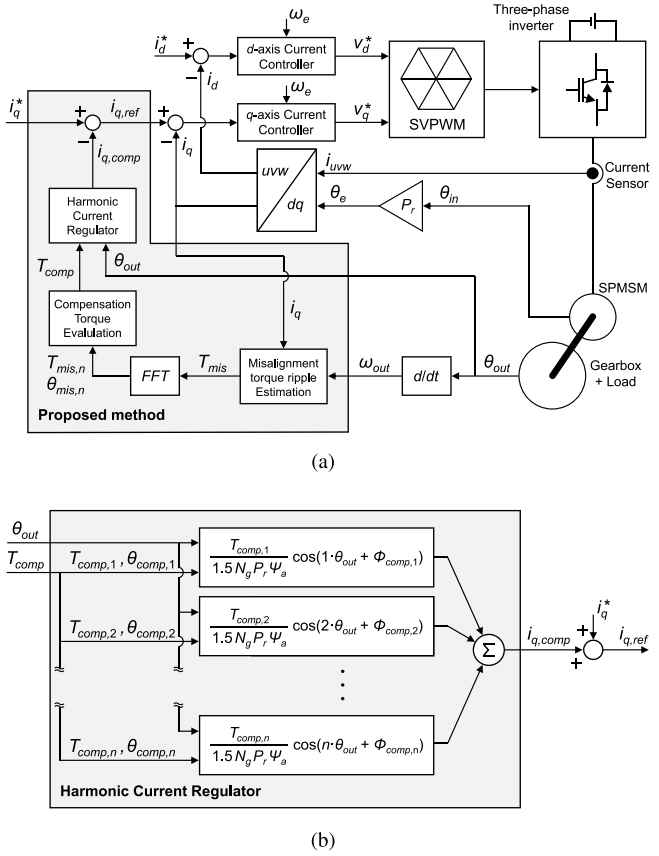

Fig. 6. Scheme of the proposed method. (a) Overall current control scheme with harmonic current injection method and (b) the harmonic current regulator.

ripple must be separated to determine the amplitude and phase of each harmonic component. The compensation torque can be expressed as

$$T_{\text{comp}} = \sum_n T_{\text{comp},n} \cos\left(n\theta_{\text{out}} + \phi_{\text{comp},n}\right) \quad (16)$$

where T_{comp} is the compensation torque, $T_{\text{comp},n}$ and $\phi_{\text{comp},n}$ are the amplitude and phase of compensation torque for the nth harmonic order, respectively.

3) Step 3: The harmonic orders of the compensation torque with components whose amplitudes of the misalignment torque ripple are greater than 20% of the maximum value are determined.
4) Step 4: The amplitude of the compensation torque is determined to be equal to the amplitude of each misalignment torque ripple. In addition, the phase of the compensation torque is determined to be opposite to that of the misalignment torque ripple. Then, the amplitude and phase of the compensation torque can be expressed as

$$T_{\text{comp},n} = T_{\text{mis},n},\ \phi_{\text{comp},n} = \phi_{\text{mis},n} + \pi \quad (17)$$

where $T_{\text{mis},n}$ and $\phi_{\text{mis},n}$ are the amplitude and phase of the misalignment torque ripple for the nth harmonic order.
5) Step 5: The compensation current, which is the sum of the harmonic currents calculated from the compensation torque, is evaluated using the harmonic current regulator. The harmonic current regulator is operated using the compensation torque, which is calculated using the estimated misalignment torque ripple, as shown in Fig. 6(a). The harmonic current regulator calculates the compensation current using the relationship between the q-axis current and electromagnetic torque, as shown in Fig. 6(b). Then, the compensation current can be expressed as

$$i_{q,\text{comp}} = \sum_n \frac{T_{\text{comp},n}}{1.5 N_g P_r \psi_a} \cos\left(n\theta_{\text{out}} + \phi_{\text{comp},n}\right) \quad (18)$$

where $i_{q,\text{comp}}$ is the compensation current.
6) Step 6: Hence, the compensation current is injected into the q-axis current command and the q-axis current reference can be expressed as follows:

$$i_{q,ref} = i_q^* + i_{q,\text{comp}} \quad (19)$$

where $i_{q,\text{ref}}$ and i_q^* are the q-axis current reference and constant q-axis current command, respectively. Finally, the q-axis current reference is transferred to the q-axis current controller, and the misalignment torque ripple is suppressed. As the friction torque and iron loss are affected by driving conditions such as load torque and rotating speed, the compensation current can be varied according to the driving conditions. Therefore, the procedure for designing the compensation current should be repeated at constant intervals.

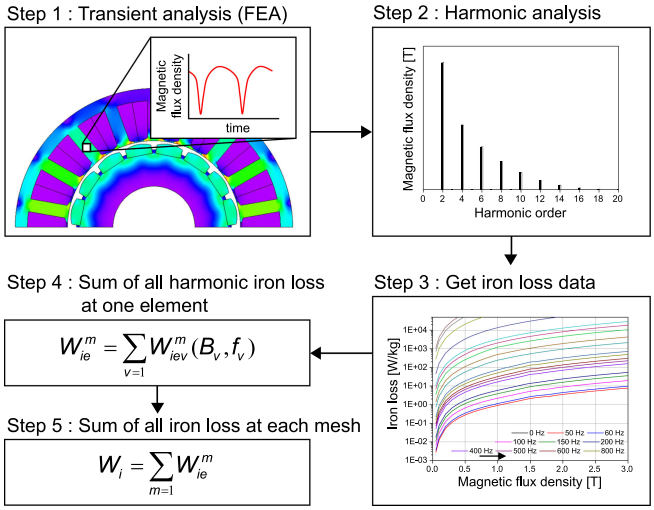

Fig. 7. Flowchart of calculating iron loss.

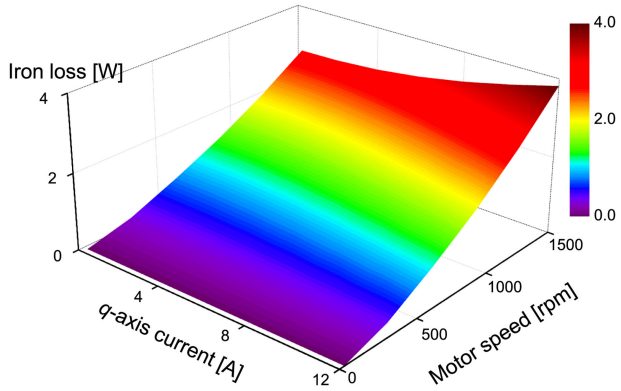

Fig. 8. Calculated iron loss according to the q-axis current and motor speed.

IV. Estimation of Misalignment Torque Ripple

The proposed harmonic current injection method can be implemented by adopting the appropriate amplitude and phase of the harmonic current. Therefore, the misalignment torque ripple should be measured to utilize the proposed method effectively. The misalignment torque ripple can be measured directly using the torque sensor; however, it is inefficient to use the torque sensor because it requires additional cost and maintenance. Thus, an indirect method for estimating the misalignment torque ripple is presented in this section. As the misalignment torque ripple is modeled as (5), the electromagnetic torque and friction coefficient must be estimated. However, the rotating speed fluctuates according to the friction torque ripple, and the fluctuation of the speed generates a fluctuation in the q-axis iron loss current. Therefore, an additional electromagnetic torque ripple is generated by the fluctuations in the iron loss. As the SPMSM is designed to have a low cogging torque and sinusoidal flux-linkage, only the electromagnetic torque ripple due to iron loss fluctuation is considered in this article.

A. Calculation of Iron Loss

The iron loss is calculated using the electromagnetic finite-element analysis (FEA) because it cannot be measured directly. The procedure for calculating the iron loss is shown in Fig. 7 [19]. First, the nonlinear FEA is performed to calculate the magnetic flux density at each mesh under certain q-axis currents and rotating speeds. Then, a harmonic analysis of the magnetic flux density is conducted to determine the amplitude at each frequency. From the iron loss data of the material, the iron loss corresponding to the magnetic flux density and frequency of each harmonic component is calculated. Then, the iron loss for each mesh is calculated by summing the iron losses of all the associated harmonic components. Consequently, the total iron loss is calculated by summing the iron losses for all the meshes. Similarly, the iron losses for each q-axis current and rotating speed are calculated repeatedly. The calculated iron loss map of the SPMSM is shown in Fig. 8. The map shows that the iron loss increases at high speeds and at high q-axis currents. Using the iron loss map, i_{cq} can be calculated according to i_q and rotating speed.

B. Estimation of Friction Coefficient

When the rotating speed is in the steady-state with constant q-axis current and constant load torque, the output torque is equal to the sum of the averaged friction torque, and load torque. Then, the friction coefficient can be calculated as

$$B = \frac{1.5 P_r \psi_a \left(i_q - \bar{i}_{\mathrm{cq}}\right) - T_l}{\bar{\omega}_{\mathrm{out}}} \tag{20}$$

where $\bar{i}_{\mathrm{cq}}$ is the averaged q-axis iron loss current. The procedure for obtaining the friction coefficient is shown in Fig. 9. When the rotating speed is in the steady state, the speed can be increased by increasing the q-axis current. As the rotating speed increases, the friction and iron loss also increase, and the rotating speed enters the steady state again. Similarly, the averaged rotating speed and q-axis current are measured from the experiments as the q-axis current increases. In addition, the iron loss current is obtained from the calculated iron loss at the corresponding rotating speed and q-axis current. As the friction torque is divided into viscous friction torque proportional to the speed and constant Coulomb friction torque, the friction coefficient can be calculated by fitting the friction torque in accordance with the averaged rotating speed. As a result, the calculated friction coefficient is 0.03654 Nm·s/rad. Then, the friction torque ripple can be obtained from the estimated friction coefficient.

C. Estimation of Misalignment Torque Ripple

The misalignment torque ripple can be estimated by substituting the electromagnetic torque ripple, which is caused by iron loss fluctuations and friction torque ripple, into (5). To verify the estimation method, the estimated misalignment torque ripple was compared with the torque ripple measured by the torque sensor, as shown in Fig. 10. The estimated torque ripple had the same order as the measured result; however, it contained errors occurred in the measurement process and while calculating the

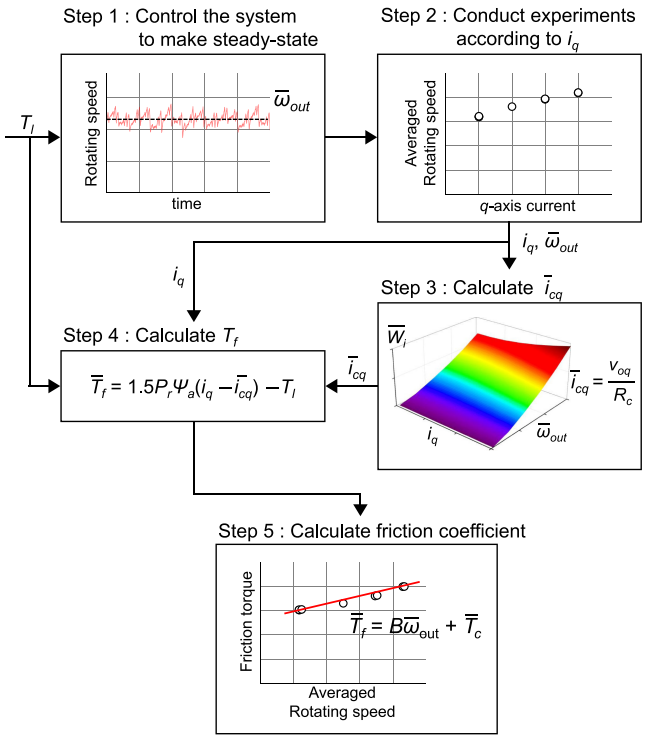

Fig. 9. Flowchart of estimating friction coefficient.

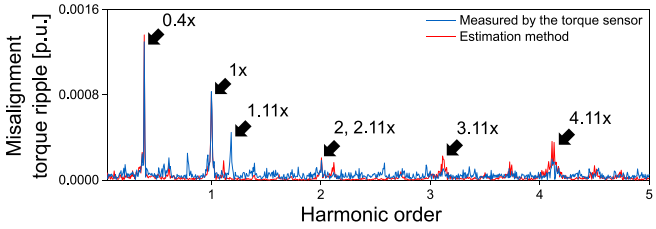

Fig. 10. Comparison of measured and estimated misalignment torque ripple.

iron loss. However, the error of 0.38th torque ripple, which has the largest amplitude, is 4.8%, thus, so that the proposed estimation method is sufficient to replace the torque sensor.

V. Experimental Verification

A. Experimental Setup

In order to use the proposed method, the SPMSM must generate low torque ripple because the torque ripple by harmonic currents should not be affected by the torque ripple of the SPMSM itself. The total harmonic distortion (THD) in back EMF can be used to analyze the harmonic components of the flux-linkage, which are responsible for causing the torque ripple. The back EMF is verified through electromagnetic FEA and experiments. In addition, the torque ripple is analyzed through electromagnetic FEA because the torque ripple of the SPMSM cannot be tested directly because of the mechanical structure of the actuator.

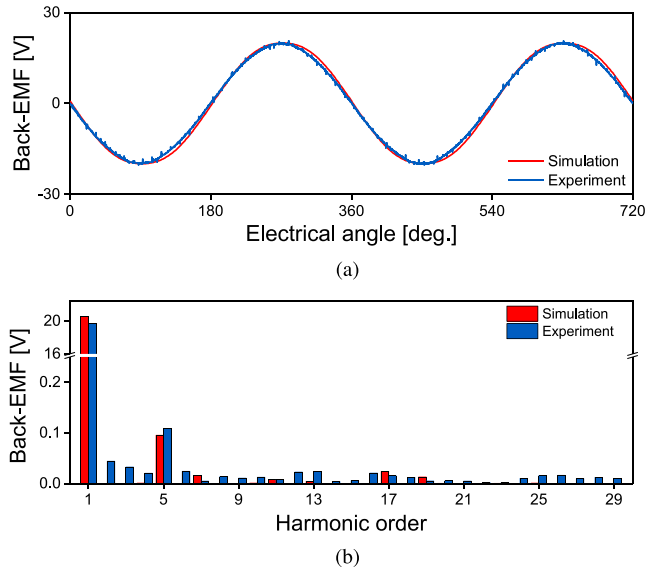

Fig. 11. Back EMF of the SPMSM. (a) Three-phase back EMF according to the electrical angle. (b) Harmonic analysis results of the back EMF.

Fig. 11(a) shows the back EMF obtained by conducting no-load electromagnetic FEA and experiments. The no-load FEA is conducted at a rotating speed of 1000 rpm. The experiment is conducted by driving the SPMSM at 1000 rpm using another servomotor. Fig. 11(b) shows the harmonic analysis results of the simulated and measured back EMF. As the stator and rotor are designed to make the back EMF sinusoidal, the SPMSM contains small harmonic components in its back EMF. The THDs of the simulated back EMF were 0.50% and 0.78%, respectively.

Fig. 12(a) shows the electromagnetic torque of the SPMSM when the sinusoidal rated current is excited, and the electromagnetic torque ripple is 2.05%. Fig. 12(b) shows the harmonic analysis results of the electromagnetic torque. As the THD of the back EMF is low, the electromagnetic torque ripple also contains low harmonic components. Therefore, the electromagnetic torque with low torque ripple can be transmitted to the gearbox.

Fig. 13 shows the experimental setup for implementing the proposed method. The actuator, torque sensor, and powder brake for load excitation are connected in series. The torque sensor is used to conduct the experiments at various load torques. The SPMSM is driven using a motor drive with an embedded digital signal processor of Texas Instrument Incorporated TMS320F28379D, and the current control loop is operated at 10 kHz. To estimate the misalignment torque ripple, the q-axis current and rotating speed are transferred from the motor drive to the PC through serial communication. As the misalignment torque ripple is calculated from the rotating speed, data should be measured over a sufficient time duration at constant sampling frequency. As the harmonic analysis is conducted using fast Fourier transform (FFT), the frequency resolution of the FFT can be determined in terms of the sampling frequency and size

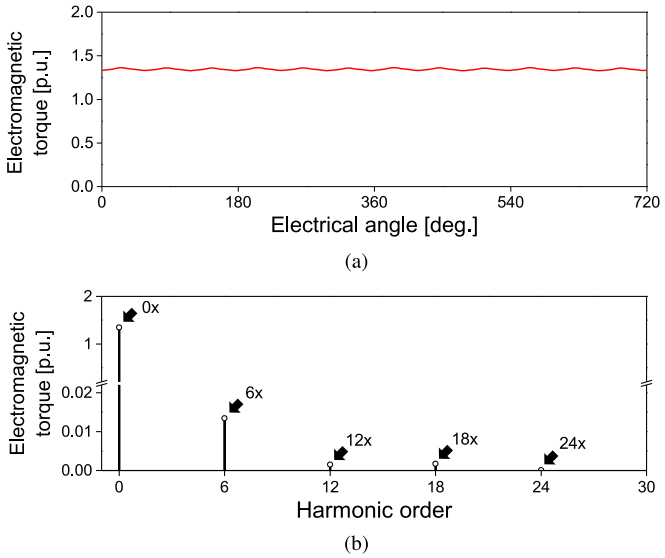

Fig. 12. Simulated electromagnetic torque of the SPMSM. (a) Electromagnetic torque according to the electrical angle. (b) Harmonic analysis result of the electromagnetic torque.

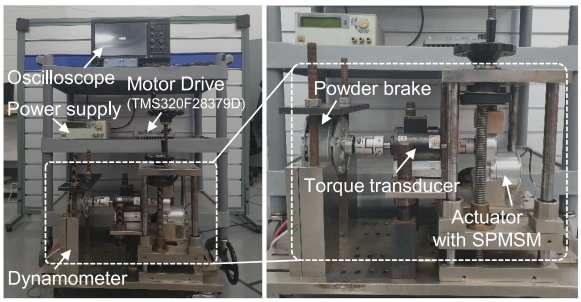

Fig. 13. Experimental setup for suppressing the misalignment torque ripple.

of FFT as

$$\Delta f = \frac{f_s}{N_{\mathrm{FFT}}} \tag{21}$$

where Δf is the frequency resolution of FFT, and f_s and N_{FFT} are the sampling frequency and size of the FFT, respectively. As the frequency of the misalignment torque ripple is close to the output rotating speed, the frequency of the compensation current is close to the frequency of the output rotating speed. As the frequency of the harmonic current is sufficiently low compared to the current control frequency of 10 kHz, the experimental setup is sufficient for generating the compensation current.

B. Experimental Verification of the Proposed Method

In this section, experiments were conducted to verify the effectiveness of the proposed method under various load conditions, as shown in Table III. The experiments were conducted under load torque of 0.125 and 0.250 p.u. where 1 p.u. is equal to the rated torque of 8 Nm, and motor speed of 0.63 p.u., where 1 p.u. is equal to the maximum motor speed of 1100 rpm. The

TABLE III
EXPERIMENTAL CONDITIONS: LOAD TORQUES AND ROTATING SPEEDS

Experiment	Load torque [p.u.]	Motor speed [p.u.]
Experiment 1	0.125	0.63
Experiment 2	0.250	0.63

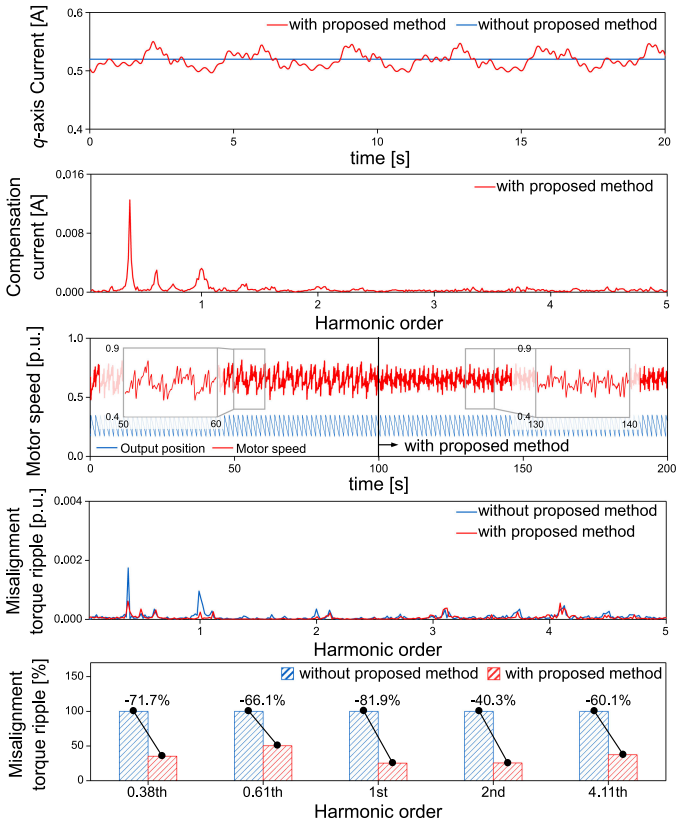

Fig. 14. Experiment 1: Waveform and FFT results of the *q-axis* current, rotating speed of input shaft, and misalignment torque ripple with/without proposed method.

experiments were conducted by the following procedure. The SPMSM is controlled with a constant q-axis current to generate a constant output torque, and the powder brake is controlled with the constant load torque. Then, the rotating speed of the output shaft is fluctuated by the misalignment torque ripple based on the averaged rotating speed. The experiments were conducted after rotating the actuator for 30 min to minimize the effect of the temperature change in the bearing and lubrication of the gearbox.

Fig. 14 compares the experimental results with/without using the proposed method. The experiment was conducted under the conditions of experiment 1 in Table III. The results show that the fluctuation of the rotating speed and misalignment torque ripple were suppressed by using the proposed method. The largest amplitude of misalignment torque ripple was measured in 0.38th harmonic order and the harmonic orders of the compensation torque were determined based on the amplitude of 0.38th harmonic order. Thus, the compensation torque includes

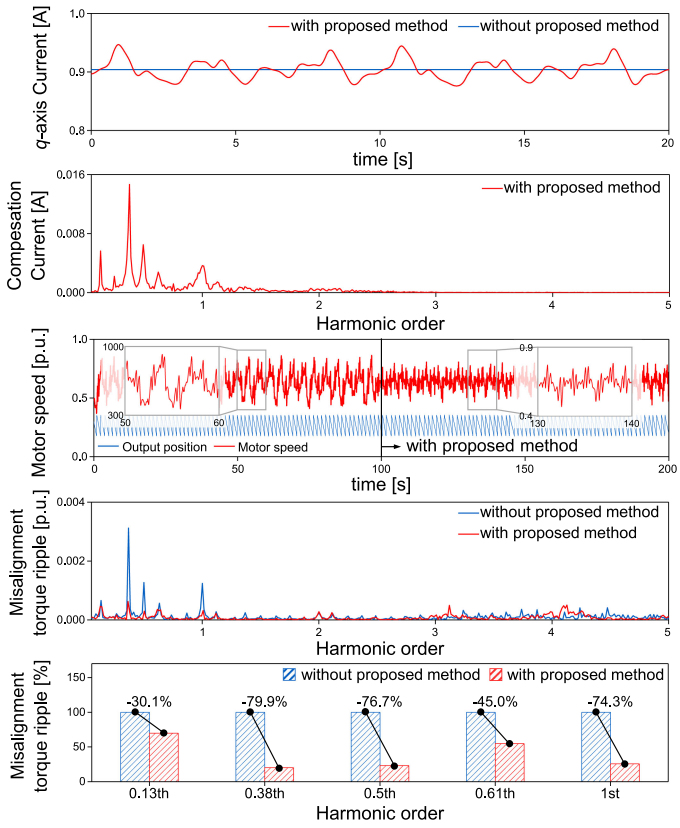

Fig. 15. Experiment 2: Waveform and FFT results of the *q-axis* current, rotating speed of input shaft, and misalignment torque ripple with/without proposed method.

the harmonic orders of 0.38th, 0.61th, 1st, 2nd, and 4.11th and the compensation current also includes the same harmonic orders. As a result of using the proposed method, the estimated misalignment torque ripple was effectively suppressed in each harmonic orders. However, it can be seen that only misalignment torque ripple of 4.11th order was selectively suppressed, this is because the misalignment torque ripple of 4.11th order is composed of several harmonic orders near in 4.11th order.

Fig. 15 show the same experimental results under the conditions of experiment 2 in Table III. It can be seen that the amplitudes of the misalignment torque ripple in each harmonic order are higher than the results of experiment 1. Since the rotating speed in experiment 2 was same as that of experiment 1, the averaged friction torque was also same for both experiments. However, the fluctuation of the iron loss current was increased as the input current increased. This causes the fluctuation of the output torque and it results to increase in the fluctuation of the rotating speed. Since the misalignment torque of experiment 2 is larger than the results of experiment 1, the amplitude of compensation current in experiment 2 is also larger than that of experiment 1. However, the estimated misalignment torque ripple were not completely suppressed because the compensation torque was calculated by using the estimation method that has error with the measured results using torque sensor.

VI. Conclusion

In this article, we proposed a method to suppress the torque ripples caused by misalignments of gearbox. The proposed method adopted the harmonic current injection method to suppress the misalignment torque ripple. In order to use the proposed method effectively, a method to estimate the misalignment torque ripple that is required to calculating the compensation torque was presented. As the misalignment torque ripple is affected by the iron loss and friction torque, the detailed process of calculating the iron loss and friction coefficient was described. The estimated misalignment torque ripple was compared with measured results obtained using a torque sensor, and the estimation method was verified to be suitable for calculating the compensation torque. Using the proposed method, the misalignment torque ripple was suppressed effectively under various load torque.

This article analyzed the feasibility of the proposed method. Based on the research results, further research on predicting the compensation currents in response to changes in driving points will be conducted.

References

[1] H. J. Park, M. S. Lim, and C. S. Lee, "Magnet shape design and verification for SPMSM of EPS system using cycloid curve," *IEEE Access*, vol. 7, pp. 137207–137216, 2019.

[2] S. W. Hwang, M. S. Lim, and J. P. Hong, "Hysteresis torque estimation method based on iron-loss analysis for permanent magnet synchronous motor," *IEEE Trans. Magn.*, vol. 52, no. 7, pp. 1–4, Jul. 2016.

[3] S. W. Hwang, J. W. Chin, M. S. Lim, and J. P. Hong, "Electromagnetic and thermal multi-physics design of SPMSM for wearable robot," in *Proc. XIII Int. Conf. Elect. Mach.*, Sep. 2018, pp. 1–7.

[4] H. Hsieh, D. Chen, L. Chien, and C. Lan, "Design of a parallel actuated exoskeleton for adaptive and safe robotic shoulder rehabilitation," *IEEE/ASME Trans. Mechatronics*, vol. 22, no. 5, pp. 2034–2045, Oct. 2017.

[5] P. Saavedra and D. Ramirez, "Vibration analysis of rotors for the identification of shaft misalignment Part 1: Theoretical analysis," in *Proc. Institution Mech. Engineers, C: J. Mech. Eng. Sci.*, vol. 218, no. 9, pp. 971–984, Sep. 2014.

[6] S. Seok *et al.*, "Design principles for energy-efficient legged locomotion and implementation on the MIT cheetah robot," *IEEE/ASME Trans. Mechatronics*, vol. 20, no. 3, pp. 1117–1129, Jun. 2015.

[7] G. H. Lee, S. I. Kim, J. P. Hong, and J. H. Bahn, "Torque ripple reduction of interior permanent magnet synchronous motor using harmonic injected current," *IEEE Trans. Magn.*, vol. 44, no. 6, pp. 1582–1585, Jun. 2008.

[8] H. Jia, M. Cheng, W. Hua, W. Zhao, and W. Li, "Torque ripple suppression in flux-switching PM motor by harmonic current injection based on voltage space-vector modulation," *IEEE Trans. Magn.*, vol. 46, no. 6, pp. 1527–1530, Jun. 2010.

[9] B. S. Lee, Z. Q. Zhu, and L. R. Huang, "Torque ripple reduction for 6-stator/4-rotor-pole variable flux reluctance machines by using harmonic field current injection," *IEEE Trans. Ind. Appl.*, vol. 53, no. 4, pp. 3730–3737, Jul./Aug. 2017.

[10] T. H. Pham, "Current harmonics injection table to minimize torque ripple for electric powertrain interior permanent magnet motor over maximum torque-speed curve," in *Proc. IEEE Transp. Electrific. Conf. Expo*, Jun. 2019, pp. 1–9.

[11] Y. B. Kim, U. Kim, D. Seok, J. So, Y. H. Lee, and H. R. Choi, "Torque sensor embedded actuator module for robotics applications," *IEEE/ASME Trans. Mech.*, vol. 23, no. 4, pp. 1662–1672, Aug. 2018.

[12] I. Godler, T. Ninomiya, and M. Horiuchi, "Ripple compensation for torque sensors built into harmonic drives," *IEEE Trans. Instrum. Meas.*, vol. 50, no. 1, pp. 117–122, Feb. 2001.

[13] M. A. Khan, I. Husain, M. R. Islam, and J. T. Klass, "Design of experiments to address manufacturing tolerances and process variations influencing cogging torque and back EMF in the mass production of the permanent-magnet synchronous motors," *IEEE Trans. Ind. Appl.*, vol. 50, no. 1, pp. 346–355, Jan./Feb. 2014.
[14] A. W. Lees, "Misalignment in rigidly coupled rotors," *J. Sound Vib.*, vol. 305, no. 1–2, pp. 261–271, Aug. 2007.
[15] J. Chacon, E. Andicoberry, V. Kappatos, G. Asfis, T. Gan, and W. Balachandran, "Shaft angular misalignment detection using acoustic emission," *Appl. Acoust.*, vol. 85, pp. 12–22, Nov. 2014.
[16] X. Liu, D. Liang, J. Du, Y. Yu, X. Yang, and Z. Luo, "Effects analysis of misalignments on dynamic characteristics test for permanent magnet synchronous motor," in *Proc. Int. Conf. Elect. Mach. Syst.*, Oct. 2014, pp. 1–5.
[17] J. Piotrowski, "Detecting misalignment on rotating machinery," in *Shaft Alignment Handbook*, 3rd ed. Boca Raton, FL, USA: CRC Press, 2007, pp. 35–87.
[18] M. Nakano, H. Kometani, and M. Kawamura, "A study on eddy-current losses in rotors of surface permanent-magnet synchronous machines," *IEEE Trans. Ind. Appl.*, vol. 42, no. 2, pp. 429–435, Mar./Apr. 2006.
[19] M. S. Lim, S. H. Chai, J. S. Yang, and J. P. Hong, "Design and verification of 150-krpm PMSM based on experimental results of prototype," *IEEE Trans. Ind. Electron.*, vol. 62, no. 12, pp. 7827–7836, Dec. 2015.

Soo-Hwan Park received the bachelor's degree in mechanical engineering, in 2014, from Hanyang University, Seoul, South Korea, where he is currently working toward the Ph.D. degree in automotive engineering.

From 2019 to 2020, he was with the Korea Institute of Industrial Technology, Cheonan-si, South Korea. His main research interests include electromagnetic field analysis, design and optimization of electric machines for automotive and robotics applications, and electric machine drive for industrial applications.

Jin-Cheol Park received the bachelor's degree in electrical engineering from Chungbuk National University, Cheongju, South Korea, in 2015, and the master's degree in automotive engineering, in 2017, from Hanyang University, Seoul, South Korea, where he is currently pursuing the Ph.D. degree in automotive engineering.

His research interests include electric machine design and drive for automotive and industrial applications.

Sung-Woo Hwang received the bachelor's degree in mechanical engineering, in 2013, from Hanyang University, Seoul, South Korea, where he is currently working toward the Ph.D. degree in automotive engineering.

His research interests include electric machine design for automotive and robot applications and numerical analysis of electromagnetics.

Jae-Hyun Kim received the bachelor's degree in mechanical engineering, in 2017, from Hanyang University, Seoul, South Korea, where he is currently working toward the Ph.D. degree in automotive engineering.

His research interests include the design, and the analysis of vibration and noise of electric machines.

Hyeon-Jin Park received the bachelor's degree in mechanical engineering, in 2011, from Hanyang University, Seoul, South Korea, where he is currently working toward the integrated master's and Ph.D. degrees in automotive engineering.

From 2014 to 2017, he was a Research Engineer with Keyang, South Korea. His research interests include electromagnetic field analysis and electric machine design.

Myung-Seop Lim (Member, IEEE) received the bachelor's degree in mechanical engineering and the master's and Ph.D. degrees in automotive engineering from Hanyang University, Seoul, South Korea, in 2012, 2014, and 2017, respectively.

From 2017 to 2018, he was a Research Engineer with Hyundai Mobis, Yongin, South Korea. From 2018 to 2019, he was an Assistant Professor with Yeungnam University, Daegu, South Korea, Since 2019, he has been with Hanyang University, Seoul, South Korea, where he is currently an Assistant Professor. His research interests include electromagnetic field analysis and electric machinery for mechatronics systems such as automotive and robot applications.